Table 1 – Clinical features of lung adenocarcinoma IA and IIIA cases.

Patient number	Gender	Smoking status	Age	Pathology					Clinical information	
				Tissue type		TNM	Lymph node involvement	Staging	Survival month	Survival status
1	M	Smoker	72	W/D ad	BAC+Pap	T1N0M0	–	IA	33	A
2	F	Non-smoker	64	W/D ad	BAC+Pap	T1N0M0	–	IA	29	A
3	M	Smoker	63	W/D ad	Pap+solid	T1N0M0	–	IA	36	A
4	F	Smoker	71	W/D ad	mucinous BAC	T1N0M0	–	IA	37	A
5	M	Non-smoker	61	W/D ad	nonmucinous BAC	T2N0M0	–	IB	16	A
6	M	Smoker	74	W/D ad	Pap	T1N0M0	–	IA	35	A
7	F	Smoker	67	W/D ad	BAC+Pap	T1N0M0	–	IA	14	A
8	M	Smoker	52	W/D ad	Pap	T2N2M0	+	IIIA	33	A
9	M	Smoker	71	P/D ad	Pap+Solid	T2N2M0	+	IIIA	19	D
10	F	Non-smoker	72	M/D ad	Pap	T2N2M0	+	IIIA	32	A
11	M	Smoker	61	P/D ad	Solid+Acinar	T2N2M0	+	IIIA	14	D
12	M	Smoker	56	P/D ad	Solid+Pap	T2N2M0	+	IIIA	20	D
13	M	Smoker	43	M/D ad	Pap+Acinar	T2N2M0	+	IIIA	15	D

NOTE: All clinical samples were retrieved from the Tokyo University Hospital. TNM is the cancer staging system that describes the extent of cancer (T, the size of the tumor; N, whether it has invaded nearby tissue regional lymph nodes that are involved; M, distant metastasis that is, spread of cancer from one body part to another). SurINS;vival months and status (A, alive or D, death) are based upon surveyed dates, April 2007. This stage IB patient was included in the IA group in semi-quantitative group comparisons between stages IA and IIIA primary tumors. Abbreviations: M, male; F, female.

83 (15.9%) proteins were uniquely identified from cancer cells spreading to the lymph nodes. However, 150 (28.8%) proteins were found to be identified in both stage IIIA primary and metastatic lesions.

Preliminary tests on MS/MS data processing suggested the parameters of both peptide and fragment mass tolerances of 2 Da and 0.8 Da [19–21] for a reasonable compromise between specificity and sensitivity of protein identifications under the

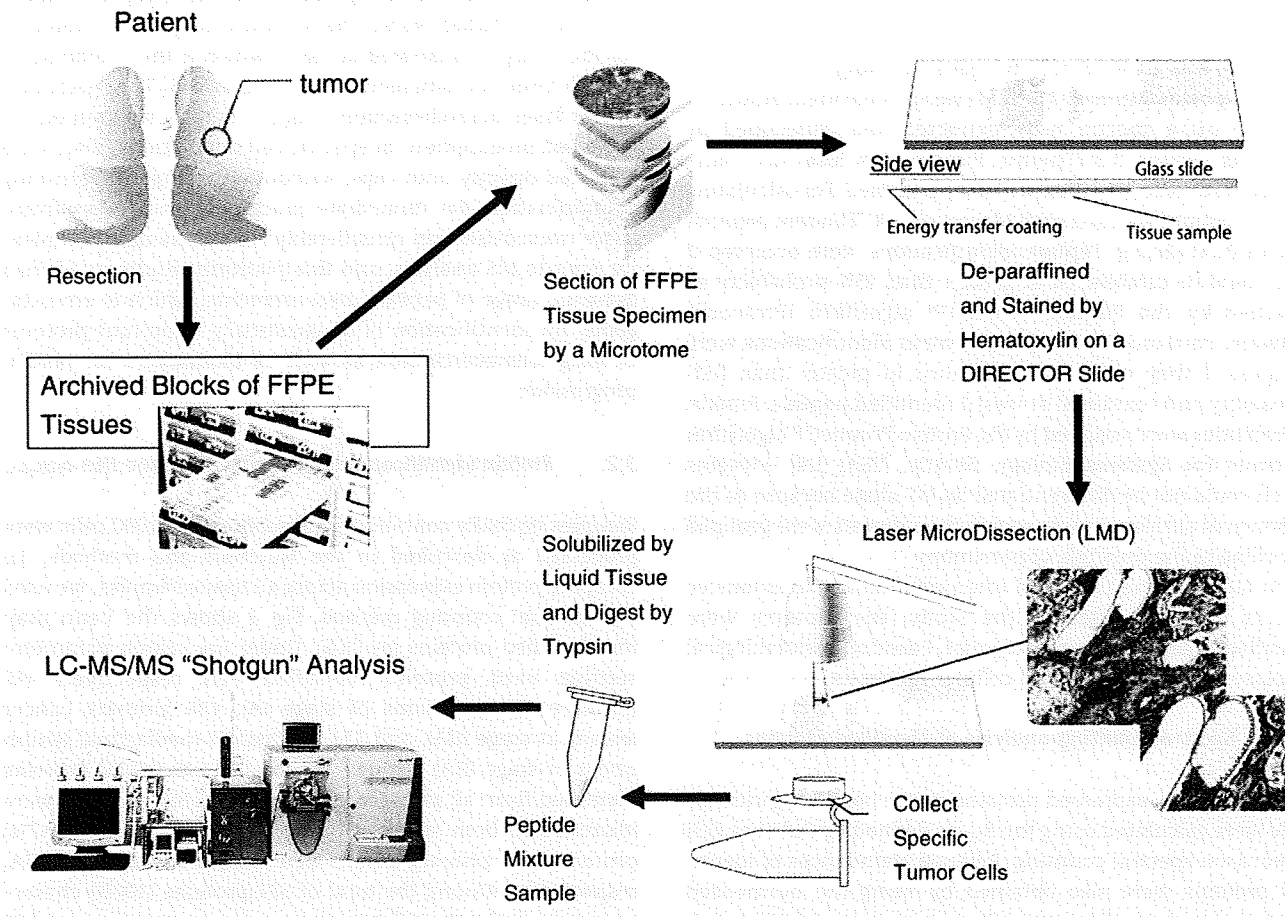

Fig. 1 – Schematic illustration of the clinical FFPE tissue proteomic screening process.

Please cite this article as: Kawamura T, et al, Proteomic analysis of laser-microdissected paraffin-embedded tissues: (1) Stage-related protein candidates upon non-metastatic lung adenocarcinoma, J Prot (2009), doi:10.1016/j.jprot.2009.11.011

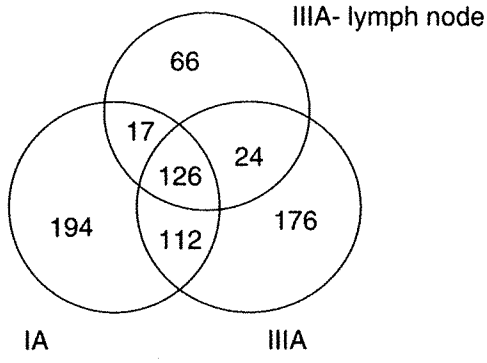

Fig. 2 – The Venn map of proteins identified from the stage IA and IIIA primary lesions and IIIA lymph node lesions.

limitations imposed by the LTQ's resolution and detection sensitivity. The use of more strict settings (peptide and fragment mass tolerances of 1.5 Da and 0.5 Da, respectively) led to a loss of a considerable number of candidate proteins, which is unfavorable for biomarker screening proteomics (Supplemental Material S3). The false-positive rates were average of 9.2 and 1.3 for the relaxed and strict settings, respectively, using a target–decoy database.

A semi-quantitative comparison of identified proteins was achieved using the spectral counting method, wherein values of R_{SC} and *NSAF* were calculated as defined in the "Materials and methods" section. [25,26] For proteins identified in stage IA and IIIA primary tumors, respectively, Fig. 3A plots each R_{SC} value against the corresponding protein (*X*-axis) in increasing order from left to right. A positive value indicates greater expression at the stage IA primary lesions, and a negative value more identified in the stage IIIA primary lesions. The graph is nearly symmetrical around its center, and the maximal R_{SC} value is about 3, which corresponds to an approximately 10-fold difference in the expression levels. In Fig. 3A, the *NSAF* value (bar) is also plotted for each corresponding protein on the *X*-axis with stage IA being above the *X*-axis and stage IIIA below. Proteins with either a high positive or negative value of R_{SC} would be candidates to characterize either stage IA or IIIA disease. Similar results were obtained in the semi-quantitative comparison of identified proteins between the stage IIIA primary and lymph node lesions as seen in Fig. 3B.

Table 2 lists the 81 proteins relevant to the primary tumors in stage IA and IIIA cases with a statistical significance of $p<0.05$ by either the *G*- or *U*-test. Representative proteins up-regulated in stage IIIA primary tumors include fatty acid synthase (FAS), heat shock 70-kDa protein 1 (HSP 70.1), calgranulin B (S100-A9), 14-3-3 protein θ (1433T), 14-3-3 protein ε (1433E), calgranulin A (S100-A8), peptidyl-prolyl cis–trans isomerase B (PPIase), heat shock protein HSP 90-α (HS90A), and anterior gradient protein 2 homolog (hAG-2). Those up-regulated in stage IA lesions were carcinoembrionic antigen-related cell adhesion molecules, tropoelastin, selenium-binding protein 1, napsin-A, cathepsin D, calmodulin, hepatoma-derived growth factor, pulmonary surfactant-associated protein B, and annexin A5. In stark contrast, was the lack of change in the levels of housekeeping proteins such as vimentin (VIME), myosin-9 (MYH9), actin-β (ACTB), type II cytokeratin-8 (K2C8) and type I cytokeratin-19 (K1C19).

Although in the semi-quantitative comparison between the primary tumors at the IIIA primary foci vs. lymph nodes 110 proteins (Supplemental Material S1) were relevant with statistical significance of $p<0.05$, very few proteins were unique to the metastatic lymph nodes were type I cytokeratin-9 (K1C9) and bromodomain adjacent to zinc finger domain 2B (hWALp4). Vimentin expression was reduced in metastatic lymph nodes, while a number of proteins, including glyceraldehyde-3-phosphate dehydrogenase (GDPTH) and actin-β, were commonly expressed and remained unchanged in both primary and metastatic lesions.

3.3. *Gene ontology analysis*

Analysis of each sample set resulted in the identification of a large number of proteins. We used bioinformatic tools to classify proteins across each of the NSCLC tumor types into different ontology categories (Fig. 4). This approach enabled the examination of the overall cellular compartment in which the identified proteins are expected to reside and function. Fig. 4 summarizes gene ontology analyses for the identified proteins. Functional annotations were counted by normalizing to the total numbers of identified proteins. Since a multifunctional protein yields more than one annotation, it results in more than 100%. The subcellular distribution of identified proteins (%) is as follows: Golgi apparatus 4.2–5.2, cytoplasm 60.4–65.5, cytoskeleton 17.6–20.6, endoplasmic reticulum 3.8–8.1, endosome 0.4–1.8, extracellular region 11.3–12.2, intracellular organelle 63.8–67.7, membrane 27.5–35.0, mitochondrion 6.7–12.9, nucleus 29.6–35.8, organelle membrane 7.9–13.5, organelle part 41.3–46.5, plasma membrane 21.9–19.2, ribosome 4.1–4.8, and unknown 6.5–10.4. The results of the molecular functions and biological processes on gene ontology analyses are shown in Supplemental Material S2.

4. Discussion

In NSCLC, the degree of metastasis is the most important factor for disease staging. Identifying pathological stage-specific proteins expression can help assess prognosis, customizing therapeutic modalities for individual patients [1–3]. In this study we explored such proteins, by global shotgun proteomics using clinically well documented microdissected FFPE tissues, and label-free spectral counting for semi-quantification. To the best of our knowledge, there had been no previous report describing successful identification of stage-specific proteins in common NSCLC lung cancers from clinical FFPE tissues.

In this study we used Mascot and a *H. sapiens* database SwissProt 55.6 (20,009 entries) for protein identification. Recent studies have indicated that the false-positive rates for the identification were statistically evaluated, using a set of nonsense peptides generated from a reverse-ordered amino acid sequence database (a decoy database). [19,28,29] We therefore pursued this statistics using two sets of mass tolerance parameters. A peptide mass tolerance and fragment mass

Please cite this article as: Kawamura T, et al, Proteomic analysis of laser-microdissected paraffin-embedded tissues: (1) Stage-related protein candidates upon non-metastatic lung adenocarcinoma, J Prot (2009), doi:10.1016/j.jprot.2009.11.011

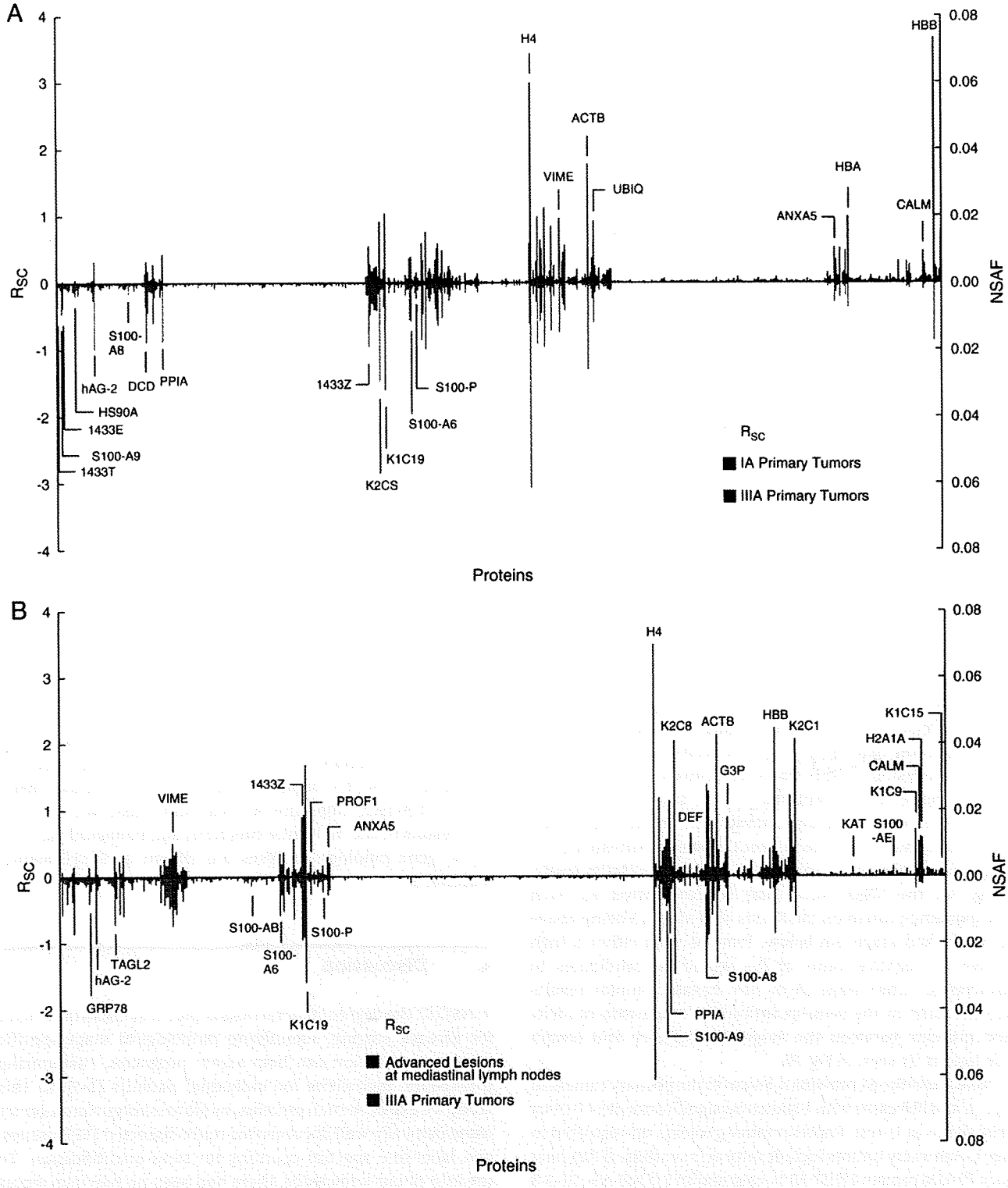

Fig. 3 – R_{SC} and *NSAF* values calculated for proteins identified (X-axis). A comparison of protein expressions: A) Stage IA *versus* IIIA primary tumors. Proteins significantly expressed in either IA or III lesions were near right or left side of X-axis. Housekeeping proteins were located around center of X-axis. B) Stage IIIA primary lesions *versus* metastatic mediastinal lymph nodes (IIIAL).

tolerance: of 2.0 and 0.8 Da, respectively (relax setting); and 1.5 and 0.5 Da, respectively (strict setting). For instruments such as the LTQ linear ion-trap mass spectrometer used in the present study, peptide mass tolerance values have usually been used in the range of 1.0–3.0 Da, depending on the complexities of analytes, machine-to-machine variations

Please cite this article as: Kawamura T, et al, Proteomic analysis of laser-microdissected paraffin-embedded tissues: (1) Stage-related protein candidates upon non-metastatic lung adenocarcinoma, J Prot (2009), doi:10.1016/j.jprot.2009.11.011

in system performance including resolution, sensitivity, and efficiency of MS/MS acquisition [19–21]. In this study, we adopted the relax setting since it provides a reasonable compromise between specificity and sensitivity of protein identifications under the limitations imposed by the resolution and detection sensitivity of our LTQ system. False-positive rates were 9.2 and 1.3 in average for the relaxed and strict settings, respectively, using the Mascot target–decoy database. The use of the strict setting decreased decoys, and concomitantly reduced the number of identified proteins to 75% of those using the relaxed one, resulting in missing a considerable number of false negative proteins, which is unfavorable for proteomic screening (Supplemental Material S3) [19–21]. In addition, we recognized in several cases that peptide ions overlapping with the second or third isotopic of another peptide ion in the high mass regions could not be measured by MS/MS using the strict setting. Consequently, plausible candidates were excluded from exploratory analysis. Even employing the strict setting, decoys still remained. However, paradoxically, 15 proteins were assigned under the strict setting not assigned under the relaxed one. This means that the strict threshold does not necessarily provide an exact identification, which seems to be caused by the nature of the software (see further Supplemental Material S3). There are no solid data upon the strict and relaxed mass tolerances in low resolution ion-trap mass spectrometry. Among 14 candidate proteins selected for further verification together with statistical tests, we demonstrated that the number of peptides identified in the strict setting was similar to that in the relaxed setting (Supplementary Material S3). Formalin fixation of tissues inevitably causes artificial modifications of proteins such as N-formylation and crosslinking by methylene bridges. Liquid Tissue™ treatment of FFPE sections and trypsin digestion, however, results in structurally informative peptides presumably derived from intact protein portions, where shotgun nanoflow-LC/MS can identify proteins [8–11]. Our results support the previous results on Liquid Tissue™ performance, and gene ontology analysis indicates that this technology can extract membrane proteins as well as soluble proteins (Fig. 4), which will be useful for clinical biomarker discovery.

Among 81 protein candidates found to be significantly related to either stage IA or IIIA primary lesions (Table 2), a subset of those proteins such as napsin-A, S100-A8, S100-A9, and hAG-2 have been investigated in their relation to malignancy and metastasis [36–39]. Napsin-A is a member of the aspartic protease family [30] and is involved in the processing of surfactant protein B (SP-B) [31]. SP-B is a critical surfactant component, and its deficiency results in fatal respiratory failure [32]. Expression of napsin was found to be associated with a high degree of differentiation in adenocarcinoma. A previous immunohistochemical study showed that napsin-A expression in primary lung adenocarcinomas can discriminate between primary and metastatic lung adenocarcinoma [33–35]. Since S100-A8, S100-A9, and hAG-2 are soluble and/or secretory proteins, they are detectable in blood, which is a property suitable for clinical biomarkers. Gene expression studies using animal models suggested that these proteins are associated with metastasis and/or formation of premetastatic niches, so-called "hot spots", in the lung [36–38].

Hiratsuka et al. [36,38] demonstrated that primary tumor cells release VEGF-A, TGF-β and TNF-α that induce the expression of the chemoattractants calgranulin A and B (S100-A8 and S100-A9) in lung endothelium in a mouse model, thereby recruiting (macrophage antigen 1)$^+$-myeloid cells and in turn facilitating the homing of tumor cells to premetastatic sites within the lung parenchyma. Both chemoattractants increase the motility of circulating cancer cells by p38-mediated activation of invasion-associated pseudopodia formation, which accelerates the assembly of the metastatic focus. These findings therefore suggest that S100-A8 and S100-A9 mediate the spread of primary cancer cells to distant sites. This study shows that the R_{SC} values for S100-A8 and S100-A9 in stage IIIA primary sites are 2.7 and 6.8 times greater, respectively than in stage IA primary sites (Fig. 3A), and that those in stage IIIA metastatic lymph nodes were 1.3 and 1.4 times, respectively, than those in stage IIIA primary tumors (Fig. 3B). Thus, our results suggest that S100-A8 and S100-A9 have increased expression in both the primary and metastatic lymph node lesions.

In the screening of breast tumor tissue using reverse transcription-PCR and immunohistochemistry with affinity-purified anti-hAG-2 antibodies, Liu et al. [39] reported that the presence of hAG-2 mRNA and protein were found to be both statistically significantly associated with estrogen alpha (ERA)-positive carcinomas and with the degree of malignancy. There were no differences in the mean latency periods of tumor formation when an expression vector bearing hAG-2 cDNA was introduced into benign rat mammary tumor cells, but metastases occurred at high rates in the lungs of animals receiving the hAG-2 transfectants (77–92% of animals with primary tumors, compared with 0% in the control groups). Their results suggest that hAG-2 is a possible marker related to cancer metastasis, which is consistent with our semi-quantitative analysis based on the spectral counting method that hAG-2 is significant in IIIA primary tumors.

5. Conclusion

We identified more than 600 proteins for stage IA and stage IIIA lung adenocarcinoma by global clinical shotgun proteomics using pathologically well-defined FFPE tissues associated with known clinical outcomes. The use of LMD to isolate tumor cells of interest reduced the complexity of subsequent LC–MS shotgun analyses to capture biomarker candidates. Evaluation by label-free spectral counting led to eighty-one candidates of potentially stage-related proteins, which are relevant to malignancy, metastasis, and prognosis. The following paper [40] describes the MRM MS quantification applied to verify a subset of those proteins, and concluded that napsin-A and anterior gradient protein 2 homolog (hAG-2) would be useful for staging IA and IIIA, which is consistent with the results obtained by this global proteomic analysis. Here we reported the first investigation using FFPE tissue specimens for the identification of stage-related biomarkers and those reflecting individual disease status, allowing personalized intervention. Thus archival FFPE tissues can be linked with reliable information concerning diagnosis and clinical outcome.

Please cite this article as: Kawamura T, et al, Proteomic analysis of laser-microdissected paraffin-embedded tissues: (1) Stage-related protein candidates upon non-metastatic lung adenocarcinoma, J Prot (2009), doi:10.1016/j.jprot.2009.11.011

Please cite this article as: Kawamura T, et al, Proteomic analysis of laser-microdissected paraffin-embedded tissues: (1) Stage-related protein candidates upon non-metastatic lung adenocarcinoma, J Prot (2009), doi:10.1016/j.jprot.2009.11.011

Table 2 – Proteins identified specifically in IA and IIIA primary tumors. (U- or G-test: $p<0.05$).

No.	Spot entry name	Accession number and description	Number of amino acids	Spectral counting			U-test		G-test	
				N_{IIIA}	N_{IA}	Fold change (R_{SC})	z-value	p-value (one tailed test)	G-score	p-value
1	1433T_HUMAN	(P27348) 14-3-3 protein theta	245	12	0	−3.4509	3.055	1.13E−03	15.970	6.44E−05
2	FAS_HUMAN	(P49327) Fatty acid synthase	2511	18	1	−3.1451	1.392	8.19E−02	18.030	2.17E−05
3	G6PD_HUMAN	(P11413) Glucose-6-phosphate 1-dehydrogenase	515	7	0	−2.7641	1.657	4.88E−02	9.060	2.60E−03
4	S10A9_HUMAN	(P06702) Calgranulin B (Migration inhibitory factor-related protein 14) (MRP-14), S100-A9	114	7	0	−2.7641	1.183	1.18E−01	9.060	2.60E−03
5	1433E_HUMAN	(P62258) 14-3-3 protein epsilon (14-3-3E)	255	13	1	−2.7079	2.695	3.52E−03	1.780	5.98E−04
6	K2C6A_HUMAN	(P02538) Keratin, type II cytoskeletal 6A (Cytokeratin-6A)	564	5	0	−2.3622	1.183	1.18E−01	4.930	2.64E−02
7	KRHB5_HUMAN	(P78386) Keratin, type II cuticular Hb5 (Hair keratin, type II Hb5)	507	5	0	−2.3622	1.183	1.18E−01	4.930	2.64E−02
8	NDRG1_HUMAN	(Q92597) NDRG1 protein (N-myc downstream-regulated gene 1 protein)	394	5	0	−2.3622	1.817	3.46E−02	4.930	2.64E−02
9	1433S_HUMAN	(P31947) 14-3-3 protein sigma (Stratifin) (Epithelial cell marker protein 1)	248	4	0	−2.1100	1.595	5.53E−02	4.930	2.64E−02
10	MARCS_HUMAN	(P29966) Myristoylated alanine-rich C-kinase substrate (MARCKS)	332	4	0	−2.1100	2.366	8.98E−03	4.930	2.64E−02
11	MYH10_HUMAN	(P35580) Myosin-10 (Myosin heavy chain, nonmuscle IIb)	1976	4	0	−2.1100	1.595	5.53E−02	4.930	2.64E−02
12	RL7_HUMAN	(P18124) 60S ribosomal protein L7	248	4	0	−2.1100	2.366	8.98E−03	4.930	2.64E−02
13	SC221_HUMAN	(O75396) Vesicle trafficking protein SEC22b	215	4	0	−2.1100	2.366	8.98E−03	4.930	2.64E−02
14	HS90A_HUMAN	(P07900) Heat shock protein HSP 90-alpha (HSP 86)	732	20	4	−2.0647	3.576	1.74E−04	11.410	7.32E−04
15	1433G_HUMAN	(P61981) 14-3-3 protein gamma (Protein kinase C inhibitor protein 1)	247	3	0	−1.8045	2.646	4.08E−03	3.560	5.90E−02
16	HNRPD_HUMAN	(Q14103) Heterogeneous nuclear ribonucleoprotein D0 (hnRNP D0)	355	3	0	−1.8045	1.732	4.16E−02	3.560	5.90E−02
17	ILF3_HUMAN	(Q12906) Interleukin enhancer-binding factor 3 (Nuclear factor of activated T-cells 90 kDa)	894	3	0	−1.8045	1.732	4.16E−02	3.560	5.90E−02
18	K1C14_HUMAN	(P02533) Keratin, type I cytoskeletal 14	472	3	0	−1.8045	1.732	4.16E−02	3.560	5.90E−02
19	K2C5_HUMAN	(P13647) Keratin, type II cytoskeletal 5	590	3	0	−1.8045	1.732	4.16E−02	3.560	5.90E−02
20	PGK2_HUMAN	(P07205) Phosphoglycerate kinase, testis specific	417	3	0	−1.8045	1.732	4.16E−02	3.560	5.90E−02
21	TCPQ_HUMAN	(P50990) T-complex protein 1 subunit theta (TCP-1-theta) (CCTtheta)	548	3	0	−1.8045	1.732	4.16E−02	3.560	5.90E−02
22	HNRPM_HUMAN	(P52272) Heterogeneous nuclear ribonucleoprotein M (hnRNP M)	730	6	1	−1.7284	1.867	3.10E−02	3.700	5.45E−02
23	HSP71_HUMAN	(P08107) Heat shock 70 kDa protein 1 (HSP70.1) (HSP70-1/HSP70-2)	641	11	3	−1.5696	2.803	2.53E−03	4.690	3.03E−02
24	PROF1_HUMAN	(P07737) Profilin-1 (Profilin I)	140	5	1	−1.5136	2.329	9.92E−03	2.690	1.01E−01
25	AGR2_HUMAN	(O95994) Anterior gradient protein 2 homolog precursor (Secreted cement gland protein XAG-2 homolog),hAG-2	175	23	8	−1.4375	1.862	3.13E−02	7.450	6.30E−03
26	A1AT_HUMAN	(P01009) Alpha-1-antitrypsin precursor (Alpha-1 protease inhibitor)	418	2	0	−1.4168	1.871	3.07E−02	2.220	1.36E−01
27	ABR_HUMAN	(Q12979) Active breakpoint cluster region-related protein	859	2	0	−1.4168	1.871	3.07E−02	2.220	1.36E−01
28	AK1A1_HUMAN	(P14550) Alcohol dehydrogenase [NADP+] (EC 1.1.1.2) (Aldehyde reductase)	325	2	0	−1.4168	1.871	3.07E−02	2.220	1.36E−01
29	ARF4_HUMAN	(P18085) ADP-ribosylation factor 4	180	2	0	−1.4168	1.871	3.07E−02	2.220	1.36E−01
30	CALL5_HUMAN	(Q9NZT1) Calmodulin-like protein 5 (Calmodulin-like skin protein)	146	2	0	−1.4168	1.871	3.07E−02	2.220	1.36E−01
31	ECHA_HUMAN	(P40939) Trifunctional enzyme alpha subunit, mitochondrial precursor	763	2	0	−1.4168	1.871	3.07E−02	2.220	1.36E−01
32	GDIR_HUMAN	(P52565) Rho GDP-dissociation inhibitor 1 (Rho-GDI 1) (Rho-GDI alpha)	204	2	0	−1.4168	1.871	3.07E−02	2.220	1.36E−01
33	I17RD_HUMAN	(Q8NFM7) Interleukin-17 receptor D precursor (IL-17 receptor D) (IL-17RD)	739	2	0	−1.4168	1.871	3.07E−02	2.220	1.36E−01
34	IGHA1_HUMAN	(P01876) Ig alpha-1 chain C region	353	2	0	−1.4168	1.871	3.07E−02	2.220	1.36E−01
35	PPIB_HUMAN	(P23284) Peptidyl-prolyl cis–trans isomerase B precursor (PPIase, Cyclophilin B)	208	2	0	−1.4168	1.871	3.07E−02	2.220	1.36E−01
36	PSME1_HUMAN	(Q06323) Proteasome activator complex subunit 1	249	2	0	−1.4168	1.871	3.07E−02	2.220	1.36E−01

37	RHG01_HUMAN	(Q07960) Rho-GTPase-activating protein 1	439	2	0	−1.4168	1.871	3.07E−02	2.220	1.36E−01
38	RL11_HUMAN	(P62913) 60S ribosomal protein L11 (CLL-associated antigen KW-12)	178	2	0	−1.4168	1.871	3.07E−02	2.220	1.36E−01
39	RL29_HUMAN	(P47914) 60S ribosomal protein L29 (Cell surface heparin-binding protein HIP)	159	2	0	−1.4168	1.871	3.07E−02	2.220	1.36E−01
40	RS9_HUMAN	(P46781) 40S ribosomal protein S9	194	2	0	−1.4168	1.871	3.07E−02	2.220	1.36E−01
41	S10A8_HUMAN	(P05109) Calgranulin A (Migration inhibitory factor-related protein 8) (MRP-8)	93	2	0	−1.4168	1.871	3.07E−02	2.220	1.36E−01
42	SEPT2_HUMAN	(Q15019) Septin-2 (Protein NEDD5)	361	2	0	−1.4168	1.871	3.07E−02	2.220	1.36E−01
43	SYCP1_HUMAN	(Q15431) Synaptonemal complex protein 1 (SCP-1)	976	2	0	−1.4168	1.871	3.07E−02	2.220	1.36E−01
44	TCP4_HUMAN	(P53999) Activated RNA polymerase II transcriptional coactivator p15	127	2	0	−1.4168	1.871	3.07E−02	2.220	1.36E−01
45	TCPG_HUMAN	(P49368) T-complex protein 1 subunit gamma (TCP-1-gamma)	545	2	0	−1.4168	1.871	3.07E−02	2.220	1.36E−01
46	UBE1_HUMAN	(P22314) Ubiquitin-activating enzyme E1 (A1S9 protein)	1058	2	0	−1.4168	1.871	3.07E−02	2.220	1.36E−01
47	DHX9_HUMAN	(Q08211) ATP-dependent RNA helicase A	1270	4	1	−1.2614	1.658	4.86E−02	1.750	1.86E−01
48	HS90B_HUMAN	(P08238) Heat shock protein HSP 90-beta (HSP 84) (HSP 90)	724	34	14	−1.2594	4.387	5.74E−06	8.500	3.50E−03
49	TBB2_HUMAN	(P07437) Tubulin beta-2 chain	444	26	11	−1.2006	1.856	3.18E−02	6.180	1.29E−02
50	LDHB_HUMAN	(P07195) L-lactate dehydrogenase B chain	334	6	2	−1.1972	1.987	2.35E−02	1.970	1.61E−01
51	ENOA_HUMAN	(P06733) Alpha-enolase (2-phospho-D-glycerate hydro-lyase)	434	34	17	−0.9983	2.360	9.13E−03	5.720	1.68E−02
52	ARF1_HUMAN	(P84077) ADP-ribosylation factor 1	181	5	2	−0.9824	2.360	9.14E−03	1.240	2.66E−01
53	PPIA_HUMAN	(P62937) Peptidyl-prolyl cis–trans isomerase A (Cyclophilin A)	165	19	10	−0.8911	2.108	1.75E−02	2.790	9.48E−02
54	ALDOC_HUMAN	(P09972) Fructose-bisphosphate aldolase C (Brain-type aldolase)	364	9	5	−0.7534	1.704	4.42E−02	1.120	2.90E−01
55	ALDOA_HUMAN	(P04075) Fructose-bisphosphate aldolase A (Lung cancer antigen)	364	15	9	−0.7059	2.189	1.43E−02	1.490	2.23E−01
56	GRP78_HUMAN	(P11021) 78 kDa glucose-regulated protein precursor (GRP 78)	654	35	22	−0.6868	1.978	2.40E−02	2.970	8.51E−02
57	K2C8_HUMAN	(P05787) Keratin, type II cytoskeletal 8	483	95	63	−0.6430	2.257	1.20E−02	6.510	1.08E−02
58	K1C19_HUMAN	(P08727) Keratin, type I cytoskeletal 19	400	85	59	−0.5733	1.483	6.90E−02	4.700	3.01E−02
59	ANXA5_HUMAN	(P08758) Annexin A5 (Annexin V)	320	12	24	0.9008	−1.160	1.23E−01	4.020	4.40E−02
60	ROA2_HUMAN	(P22626) Heterogeneous nuclear ribonucleoproteins A2/B1	353	9	24	1.2732	−2.489	6.40E−03	6.970	8.30E−03
61	HBA_HUMAN	(P69905) Hemoglobin alpha subunit (Hemoglobin alpha chain) (Alpha-globin)	142	7	20	1.3362	−2.082	1.87E−02	6.410	1.14E−02
62	PTMA_HUMAN	(P06454) Prothymosin alpha [Contains: Thymosin alpha-1]	111	1	5	1.4395	−1.719	4.28E−02	2.690	1.01E−01
63	ALDH2_HUMAN	(P05091) Aldehyde dehydrogenase, mitochondrial precursor	517	3	11	1.4953	−1.285	9.95E−02	4.690	3.03E−02
64	ATPB_HUMAN	(P06576) ATP synthase beta chain, mitochondrial precursor	529	6	20	1.5233	−2.240	1.25E−02	7.800	5.20E−03
65	PSPB_HUMAN	(P07988) Pulmonary surfactant-associated protein B precursor (SP-B)	381	1	6	1.6542	−1.876	3.03E−02	3.700	5.45E−02
66	CO6A3_HUMAN	(P12111) Collagen alpha-3(VI) chain precursor	3176	0	3	1.7304	−2.121	1.69E−02	3.560	5.90E−02
67	HDGF_HUMAN	(P51858) Hepatoma-derived growth factor (HDGF)	240	0	3	1.7304	−2.121	1.69E−02	3.560	5.90E−02
68	CALM_HUMAN	(P62158) Calmodulin (CaM)	149	2	10	1.7595	−2.135	1.64E−02	5.590	1.81E−02
69	FRIL_HUMAN	(P02792) Ferritin light chain (Ferritin L subunit)	175	1	7	1.8413	−0.973	1.65E−01	4.760	2.91E−02
70	NAPSA_HUMAN	(O96009) Napsin-A precursor (Napsin-1) (NAPA) (TA01/TA02)	420	1	7	1.8413	−1.508	6.58E−02	4.760	2.91E−02
71	CATD_HUMAN	(P07339) Cathepsin D precursor	412	0	4	2.0359	−1.922	2.73E−02	4.930	2.64E−02
72	HNRCL_HUMAN	(O60812) Heterogeneous nuclear ribonucleoprotein C-like 1	293	0	4	2.0359	−2.828	2.34E−03	4.930	2.64E−02
73	NPM_HUMAN	(P06748) Nucleophosmin (NPM) (Nucleolar phosphoprotein B23) (Numatrin)	294	0	4	2.0359	−1.922	2.73E−02	4.930	2.64E−02
74	SBP1_HUMAN	(Q13228) Selenium-binding protein 1	472	0	4	2.0359	−1.333	9.12E−02	4.930	2.64E−02
75	VINC_HUMAN	(P18206) Vinculin (Metavinculin)	1134	0	4	2.0359	−1.922	2.73E−02	4.930	2.64E−02
76	HBB_HUMAN	(P68871) Hemoglobin beta subunit (Hemoglobin beta chain) (Betaglobin)	147	17	77	2.1022	−2.337	9.72E−03	41.230	1.35E−10
77	DHCA_HUMAN	(P16152) Carbonyl reductase [NADPH] 1	277	1	10	2.2907	−1.107	1.34E−01	8.180	4.20E−03
78	MDHM_HUMAN	(P40926) Malate dehydrogenase, mitochondrial precursor	338	1	10	2.2907	−2.797	2.58E−03	8.180	4.20E−03
79	ELN_HUMAN	(P15502) Elastin precursor (Tropoelastin)	786	0	8	2.8556	−2.489	6.41E−03	10.440	1.20E−03
80	CEAM6_HUMAN	(P40199) Carcinoembryonic antigen-related cell adhesion molecule 6 precursor	344	0	9	3.0044	−2.274	1.15E−02	11.820	5.86E−04
81	HBD_HUMAN	(P02042) Hemoglobin delta subunit	147	0	16	3.7599	−1.246	1.06E−01	21.510	3.52E−06

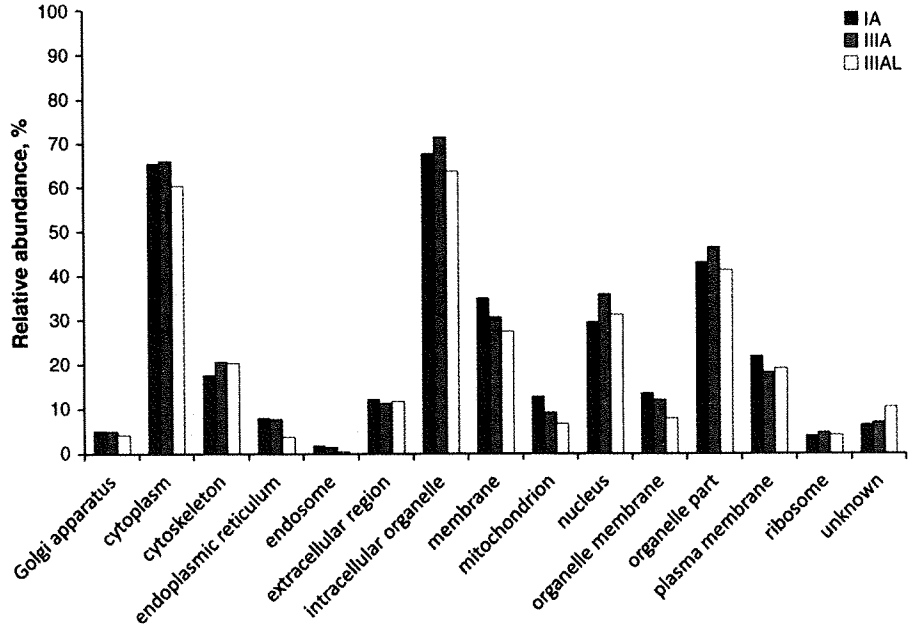

Fig. 4 – Gene ontology (GO) on cellular compartment for proteins identified from lung adenocarcinoma stage IA and IIIA primary tumors (IA and IIIA) and metastatic mediastinal lymph nodes (IIIAL).

Acknowledgments

We thank Dr. David Krizman (Expression Pathology, Gaithersburg, MD, USA) for technical discussion on the Liquid Tissue™ protocol/reagents and the Director™ slides. We are also gratefully for financial support from the 3rd Cancer Broad Strategic Project of the Japanese Ministry of Public Welfare and Labor.

Appendix A. Supplementary data

Supplementary data associated with this article can be found, in the online version, at doi:10.1016/j.jprot.2009.11.011.

REFERENCES

[1] Mountain CF. Revisions in the international system for staging lung cancer. Chest 1997;111:1710–7.
[2] Asamura H, Goya T, Koshiishi Y, Sohara Y, Eguchi K, Mori M, et al. A Japanese Lung Cancer Registry study: prognosis of 13,010 resected lung cancers. J Thorac Oncol 2008;3:46–52.
[3] Herbst RS, John V, Heymach JV, Lippman SM. Lung Cancer. N Engl J Med 2008;359:367–80.
[4] Pazdur R, Wagman LD, Camphausen KA, Hoskins W. Cancer management: a multidisciplinary approach11th Edition. 2008. p. 114.
[5] Shi SR, Cote RJ, Taylor CR. Antigen retrieval immunohistochemistry: past, present, and future. J Histochem Cytochem 1997;45:327–43.
[6] Tourtellotte WW, Verity AN, Schmid P, Martinez S, Shapshak P. Covalent binding of formalin fixed paraffin embedded brain tissue sections to glass slides suitable for in situ hybridization. J Virol Methods 1987;15:87–99.
[7] Zhao J, Wu R, Au A, Marquez A, Yu Y, Shi Z. Determination of HER2 gene amplification by chromogenic in situ hybridization (CISH) in archival breast carcinoma. Mod Pathol 2002;15:657–65.
[8] Prieto DA, Hood BL, Darfler MM, Guiel TG, Lucas DA, Conrads TP, et al. Liquid Tissue™: proteomic profiling of formalin-fixed tissues. BioTechniques 2005;38:S32–5.
[9] Hood BL, Darfer MM, Furusato B, Lucas DA, Ringeisen BR, Sesterhenn IA, et al. Proteomic analysis of formalin-fixed prostate cancer tissue. Mol Cell Proteomics 2005;4:1741–53.
[10] Hood BL, Conrads TP, Veenstra TD. Unravelling the proteome of formalin-fixed paraffin-embedded tissue. Brief Funct Genomic Proteomic 2006;5:169–75.
[11] 3THood BL, Conrads TP, Veenstra TD. Mass spectrometric analysis of formalin-fixed paraffin-embedded tissue: Unlocking the proteome within. Proteomics 2006;6:4106–14.
[12] Mueller LN, Brusniak MY, Mani DR, Aebersold R. An assessment of software solutions for the analysis of mass spectrometry based quantitative proteomics data. J Proteome Res 2008;7:51–61.
[13] Ronci M, Bonanno E, Colantoni A, Pieroni L, Di Ilio C, Spagnoli LG, et al. Protein unlocking procedures of formalin-fixed paraffin-embedded tissues: application to MALDI-TOF imaging MS investigations. Proteomics 2008;8:3702–14.
[14] Overton WR, Catalano E, McCoy Jr JP. Method to make paraffin-embedded breast and lymph tissue mimic fresh tissue in DNA analysis. Cytometry 1996;26:166–71.
[15] Xie H, Griffin TJ. Trade-off between high sensitivity and increased potential for false positive peptide sequence matches using a two-dimensional linear ion trap for tandem mass spectrometry-based proteomics. J Proteome Res 2006;5:1003–9.
[16] Fujii K, Nakano T, Kanazawa M, Akimoto S, Hirano T, Kato H, et al. Clinical-scale high-throughput human plasma proteome analysis: lung adenocarcinoma. Proteomics 2005;5:1150–9.
[17] Fujii K, Nakano T, Hike H, Usui F, Bando Y, Tojo H, et al. Fully automated online multi-dimensional protein profiling

Please cite this article as: Kawamura T, et al, Proteomic analysis of laser-microdissected paraffin-embedded tissues: (1) Stage-related protein candidates upon non-metastatic lung adenocarcinoma, J Prot (2009), doi:10.1016/j.jprot.2009.11.011

system for complex mixtures. J Chromatogr A 2004;1057:107–13.
[18] Perkins DN, Pappin DJ, Creasy DM, Cottrell JS. Probability-based protein identification by searching sequence databases using mass spectrometry data. Electrophoresis 1999;20:3551–67.
[19] Elias JE, Haas W, Faherty BK, Gygi SP. Comparative evaluation of mass spectrometry platforms used in large-scale proteomics investigations. Nat Methods 2005;2:667–75.
[20] Patwardhan AJ, Strittmatter EF, Camp II DG, Smith RD, Palavicini MG. Comparison of normal and breast cancer cell lines using proteome, genome, and interactome data. J Proteome Res 2005;4:1952–60.
[21] Orosch M, Swamy S, Hubbard T, Choudhary J. Comparison of Mascot and X!Tandem performance for low and high accuracy mass spectrometry and the development of an adjusted Mascot threshold. Mol Cell Proteomics 2008;7:962–70.
[22] Craig R, Beavis RC. TANDEM: matching proteins with tandem mass spectra. Bioinformatics 2004;20:1466–7.
[23] Craig R, Beavis RC. A method for reducing the time required to match protein sequences with tandem mass spectra. Rapid Commun Mass Spectrom 2003;17:2310–6.
[24] Chen SS, Deutsch EW, Yi EC, Li X-j, Goodlett DR, Aebersold R. Improving mass and liquid chromatography based identification of proteins using Bayesian scoring. J Proteome Res 2005;4:2174–84.
[25] Old WM, Meyer-Arendt K, Aveline-Wolf L, Pierce KG, Mendoza A, Sevinsky JR, et al. Comparison of label-free methods for quantifying human proteins by shotgun proteomics. Mol Cell Proteomics 2005;4:1487–502.
[26] Zybailov B, Coleman MK, Florens L, Washburn MP. Correlation of relative abundance ratios derived from peptide ion chromatograms and spectrum counting for quantitative proteomic analysis using stable isotope labeling. Anal Chem 2005;77:6218–24.
[27] Sokal RR, Rohlf FJ. Biometry: the principles and practice of statistics in biological research. New York: W.H. Freeman; 1995. p. 729–31.
[28] Kall L, Storey JD, MacCoss MJ, Noble WS. Assigning significance to peptides identified by tandem mass spectrometry using decoy databases. J Proteome Res 2008;7:29–34.
[29] Wang G, Wu WW, Zhang Z, Masilamani S, Shen RF. Decoy methods for assessing false positives and false discovery rates in shotgun proteomics. Anal Chem 2009;81:146–59.
[30] Ueno T, Elmberger G, Weaver TE, Toi M, Linder S. The aspartic protease napsin A suppresses tumor growth independent of its catalytic activity. Lab Invest 2008;88:256–63.
[31] Brasch F, Ochs M, Kahne T, Guttentag S, Schauer-Vukasinovic V, Derrick M, et al. Involvement of napsin A in the C- and N-terminal processing of surfactant protein B in type-II pneumocytes of the human lung. J Biol Chem 2003;278:49006–14.
[32] Ueno T, Linder S, Elmberger G. Aspartic proteinase napsin is a useful marker for diagnosis of primary lung adenocarcinoma. Br J Cancer 2003;88:1229–33.
[33] Jagirdar J. Application of immunohistochemistry to the diagnosis of primary and metastatic carcinoma to the lung. Arch Pathol Lab Med 2008;132:384–96.
[34] Chuman Y, Bergman A, Ueno T, Saito S, Sakaguchi K, Alaiya AA, et al. Napsin A, a member of the aspartic protease family, is abundantly expressed in normal lung and kidney tissue and is expressed in lung adenocarcinomas. FEBS Lett 1999;462:129–34.
[35] Dejmek A, Naucler P, Smedjeback A, Kato H, Maeda M, Yashima K, et al. Napsin A (TA02) is a useful alternative to thyroid transcription factor-1 (TTF-1) for the identification of pulmonary adenocarcinoma cells in pleural effusions. Diagn Cytopathol 2007;35:493–7.
[36] Hiratsuka S, Watanabe A, Aburatani H, Maru Y. Tumour-mediated lung metastasis. Nat Cell Biol 2006;8:1369–75.
[37] Rafii S, Lyden D. S100 chemokines mediate bookmarking of premetastatic niches. Nat Cell Biol 2006;8:1321–3.
[38] Hiratsuka S, Watanabe A, Sakurai Y, Akashi-Takamura S, Ishibashi S, Miyake K, Shibuya M, Akira S, Aburatani H, Maru Y. The S100A8-serum amyloid A3-TLR4 paracrine cascade establishes a pre-metastatic phase. Nat Cell Biol 2008;10:1349–55.
[39] Liu D, Rudland PS, Sibson DR, Platt-Higgins A, Barraclough R. Human homologue of cement gland protein, a novel metastasis inducer associated with breast carcinomas. Cancer Res 2005;65:3796–805.
[40] Nishimura T, Nomura M, Tojo M, Hamasaki H, Fukuda T, Fujii K, et al. Proteomic analysis of laser-microdissected paraffin-embedded tissues: (2) MRM assay for stage-related proteins upon non-metastatic lung adenocarcinoma. To be published as the following article in Journal of Proteomics, this volume. doi:10.1016/j.jprot.2009.11.011.

Please cite this article as: Kawamura T, et al, Proteomic analysis of laser-microdissected paraffin-embedded tissues: (1) Stage-related protein candidates upon non-metastatic lung adenocarcinoma, J Prot (2009), doi:10.1016/j.jprot.2009.11.011

JOURNAL OF PROTEOMICS XX (2009) XXX–XXX

available at www.sciencedirect.com

ScienceDirect

www.elsevier.com/locate/jprot

Journal of PROTEOMICS

Proteomic analysis of laser-microdissected paraffin-embedded tissues: (2) MRM assay for stage-related proteins upon non-metastatic lung adenocarcinoma

Toshihide Nishimura[a,*,1], *Masaharu Nomura*[a,1], *Hiromasa Tojo*[b], *Hiroko Hamasaki*[c], *Tetsuya Fukuda*[d], *Kiyonaga Fujii*[e], *Sayaka Mikami*[d], *Yasuhiko Bando*[d], *Harubumi Kato*[a]

[a]*Department of Surgery, Tokyo Medical University, Shinjuku, Tokyo, Japan*
[b]*Department of Biophysics and Biochemistry, Osaka University Graduate School of Medicine, Osaka, Japan*
[c]*Department of Biomedical Science, Graduate School of Agricultural and Life Sciences, The University of Tokyo, Tokyo, Japan*
[d]*Biosys Technologies, Inc., Meguro, Tokyo, Japan*
[e]*Department of Structural Biology, Graduate School of Pharmaceutical Sciences, Hokkaido University, Sapporo, Japan*

ARTICLE INFO

Article history:
Received 29 September 2009
Accepted 16 November 2009

Keywords:
Formalin-fixed paraffin-embedded tissues
Lung adenocarcinoma
Non-small cell lung cancer
Mass spectrometry
Multiple-reaction monitoring

ABSTRACT

A preceding paper suggested 81 candidates of stage-specifically expressed proteins for either stage IA or IIIA by global shotgun proteomics and spectral counting. Six proteins, a subset of these proteins, were chosen for a further verification study since they are potentially soluble and/or secretory, which nature is convenient for detecting them in blood in clinical practice. The multiple-reaction monitoring (MRM) quantitative analysis suggested that napsin-A and anterior gradient protein 2 homolog (hAG-2) out of the 6 candidates would be useful for determining stage IA or IIIA and are related to metastasis. In the study we noted that stage IIIA patients with better outcome showed napsin-A profiles similar to that of stage IA patients. We therefore examined 14 additional patients for analysis, which contained the IA-stage patients of poorer outcome and the IIIA-stage patients of better outcome. The MRM analysis of napsin-A for all patients suggests that napsin-A contents correlate with better outcome in stage IA. This and discovery studies demonstrate that direct isolation of tumor cells alone by laser microdissection (LMD) greatly reduces complexity on comprehensive analyses, and that MRM mass spectrometry using the endogenous internal standard is a feasible technology for quantitative verification of target proteins in formalin-fixed paraffin embedded (FFPE) tissues.

1. Introduction

Lung cancer is one of the leading causes of cancer-related death, and lung adenocarcinoma is common among non-small cell lung cancers (NSCLCs), which group also includes squamous cell carcinoma and large cell carcinoma [1,2]. The staging of the disease is closely related to prognosis, and the degree of mediastinal lymph node (MLN) involvement is a decisive component in the staging process. This offers no previous investigation on biomarker discovery/verification of

Abbreviations: FFPE, formalin-fixed and paraffin-embedded; ISIS, in-sample internal standard; LC, liquid chromatography; LMD, laser microdissection; MIDAS, MRM-initiated detection and sequencing; MLN, mediastinal lymph node; MRM, multiple-reaction monitoring; MS, mass spectrometry; MS/MS, tandem mass spectrometry; NSCLC, non-small cell lung cancer.

* *Corresponding author.* Tel.: +81 90 9823 5442; fax: +81 33340 0960.
E-mail address: linne300@aol.com (T. Nishimura).
[1] Contributed equally.

1874-3919/$ – see front matter © 2009 Elsevier B.V. All rights reserved.
doi:10.1016/j.jprot.2009.11.010

Please cite this article as: Nishimura T, et al, Proteomic analysis of laser-microdissected paraffin-embedded tissues: (2) MRM assay for stage-related proteins upon non-metastatic lung adenocarcinoma, J Prot (2009), doi:10.1016/j.jprot.2009.11.010

lung cancer utilizing FFPE tissue materials. FFPE tissue specimens are usually stored in hospitals for decades and are huge untapped information resources regarding disease progression as well as drug response and toxicity. Another advantage in using FFPE tissues is that the clinical outcomes of the patients are usually already known. Laser microdissection (LMD) of FFPE tissue is a powerful methodology, because it can separate cells directly relevant to the disease from adjacent normal cells, since diseased and adjacent normal or interstitial tissues are often intermingled [3–6].

Mass spectrometry-based MRM assay is a powerful method that measures the amount of a specific peptide sequence, resulting in highly selective and sensitive quantification of candidate proteins, by which a multiplex protein assay can be performed within a single run while an antibody-based approach can be problematic. This MRM MS-based analysis was conducted to verify the subset of candidate proteins determined in a preceding study [12]. Fig. 1 illustrates the schematic workflow of LC-MRM MS-based verification assay. MRM measurements have long been used for pharmacokinetic/pharmacodynamic analysis of small molecule drugs in plasma. Anderson and Hunter [7] clearly demonstrated the potential of quantitative MRM assay for multiplex, plasma-based polypeptide biomarker profiling, using a hybrid triple quadrupole linear ion trap (IT) mass spectrometer. In a triple quadrupole mass spectrometer, Q1 is set to transmit precursor ions of the defined mass-to-charge ratio (*m/z*), while Q3 is set to selectively transmit ions of the *m/z* for a specific/diagnostic product ion resulting from collision-induced dissociation (CID). MRM measurements are particularly useful for specific analysis of a target within complex mixtures due to this two stage mass selection [7–9]. In this study we designed MRM transitions for a subset of candidate proteins obtained in a preliminary study [12] using the results from an empirical LC-MS/MS survey and a semi-empirical approach and MRM-initiated detection and sequencing (MIDAS) [10,11] that combines *in silico* prediction of precursor and fragment masses and experimental (MS/MS) survey strategy.

2. Materials and methods

2.1. FFPE tissue samples

Archived FFPE samples were obtained from a total of 13 resected lung cancer patients between 1997 and 2004 at the Tokyo Medical University Hospital and were retrieved with the

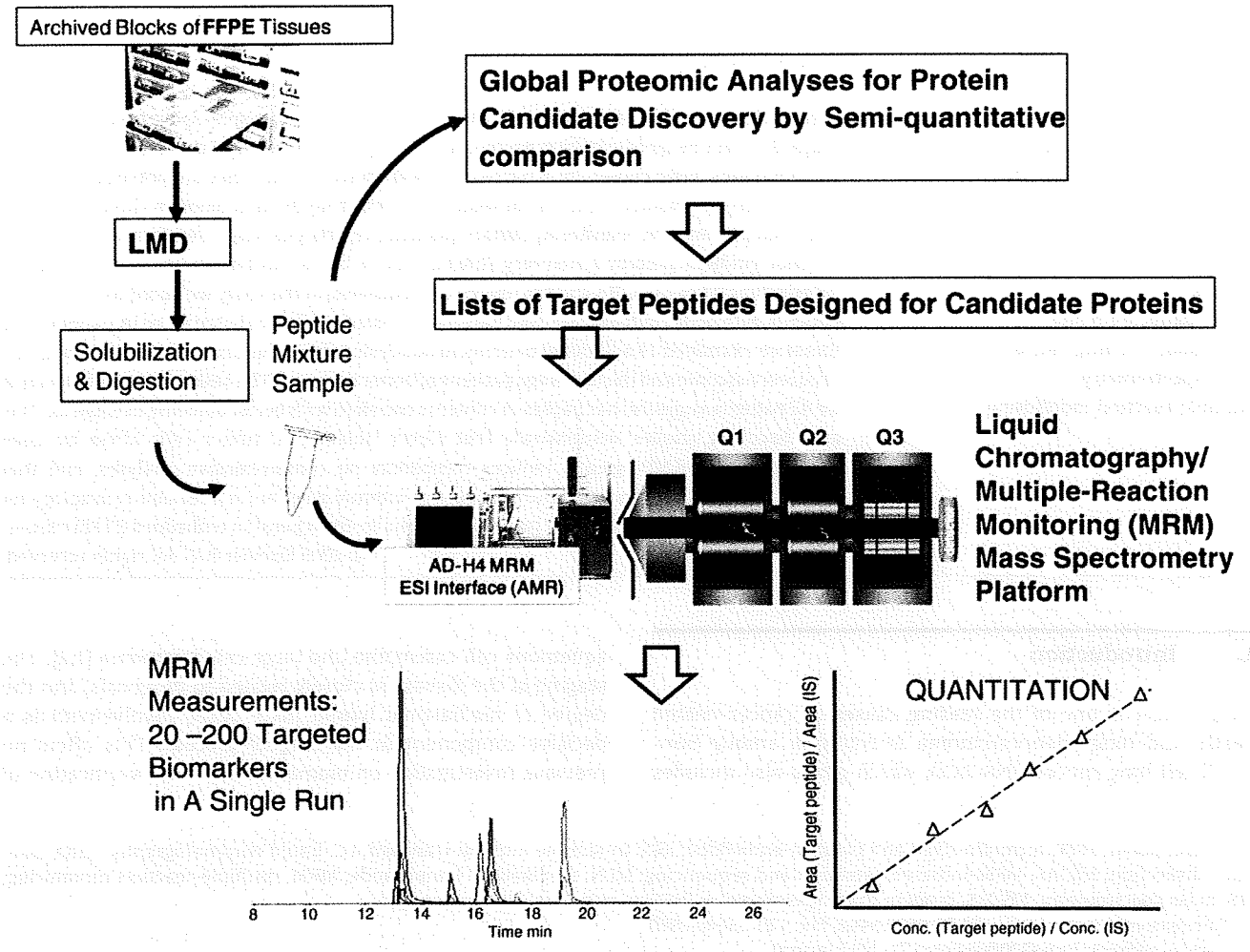

Fig. 1 – A schematic illustration of the liquid chromatography-MRM MS verification assay. A peptide-mixture sample prepared from a laser-microdissected FFPE tissue following Liquid Tissue solubilization and tryptic digestion was subjected to LC-MRM MS analysis by which multiple peptides designed for candidate proteins are in principle quantified in a single run.

Please cite this article as: Nishimura T, et al, Proteomic analysis of laser-microdissected paraffin-embedded tissues: (2) MRM assay for stage-related proteins upon non-metastatic lung adenocarcinoma, J Prot (2009), doi:10.1016/j.jprot.2009.11.010

approval of the Ethical Committee of the hospital. Those patients were the same as in the discovery study [12], and were used for validation of the results of global shotgun proteomics by MRM mass spectrometry. To examine the relationship between disease prognosis and two stage IA-related candidates (napsin-A and tropoelastin) [12], we examined 14 additional patients, including unexpected outcome patients for their stage, i.e., IA-stage patients with poor outcome and IIIA-stage patients with good outcome. Table 1 shows the summary of patient profiles. Reagents, laser microdissection (LMD) and Liquid Tissue™ solubilization method (see protocols in http://www.expressionpathology.com/) were described in the preceding paper [12].

2.2. LC-MRM analysis

The capillary reversed-phase μ-LC-MS/MS system comprised a Paradigm MS4 dual solvent delivery system (Michrom BioResources, Auburn, CA, USA) connected to a hybrid triple quadrupole/linear ion trap mass spectrometer (4000-QTRAP, Applied Biosystems/MDSciex, Foster City, CA, USA) operating in the positive ion mode [7]. A 2.5-μL aliquot of each sample (0.25–0.5 μg total peptide) was desalinated on line with an L-trap micro cartridge 0.3 mm in length (Chemicals Evaluation Research Institute, Tokyo, Japan) fitted to the autosampler HTC-PAL injector valve (CTC Analytics, Zwingen, Switzerland), which had been pre-equilibrated with 0.1% trifluoroacetic acid (aq.) containing 2% acetonitrile. After switching the valve, peptides were loaded on a capillary reversed-phase column (0.1×150 mm) packed with MAGIC C18 AQ (3 μm in diameter, and 100-Å pore size; Michrom BioResources) for separation. Mobile phase A was 98% water/2% acetonitrile/0.1% formic acid, and mobile phase B was 10% water/90% acetonitrile/0.1% formic acid. Peptides were eluted from the column with a linear gradient from 95:5; mobile phase A/mobile phase B to 15:85; mobile phase A/mobile phase B over 60 min at a flow rate of 500 nL/min. The LC eluent was subjected to positive ion nanoflow analysis using a NanoSpray II source (Applied Biosystems/MDSciex). The column eluent was directed into the MicroIonSpray II spray head *via* coupling to a distal coated PicoTip fused silica spray tip (360 μm o.d., 50 μm i.d., 10 μm emitter orifice; New Objective, Woburn, MA, USA). Samples were analyzed with an ionspray voltage of 2.5 kV, heater interface temperature of 150 °C, curtain gas flow of 10 and nebulizing gas flow of 5. For all MRM studies, quadrupoles were operated in the unit/unit resolution, the dwell times 50 ms, and collision energy

Table 1 – Patient characteristics and clinical features.

Staging	Patient number	Gender	Age	Histologic type[a]	Survival months	Present status[b]
A. Validation						
IA	1	M	72	W	33	A
	2	F	64	W	29	A
	3	M	63	W	36	A
	4	F	71	W	37	A
	5	M	61	W	16	A
	6	M	74	W	35	A
	7	F	67	W	14	A
IIIA	8	M	43	M	15	D
	9	M	71	P	19	D
	10	M	61	P	14	D
	11	M	56	P	20	D
	12	M	52	W	33	A
	13	F	72	M	32	A
B. Additional patients						
IA	14	F	68	M	63	A
	15	F	74	W	62	A
	16	M	75	P	11	D
	17	F	77	P	10	D
	18	F	65	W	34	D
	19	M	56	M	19	D
	20	F	69	W	60	D
IIIA	21	F	74	P	13	D
	22	F	27	M	49	D
	23	F	71	M	23	D
	24	F	69	P	13	D
	25	F	65	M	9	D
	26	F	66	M	102	A
	27	F	68	M	74	A

[a] W, well differentiated; M, moderately differentiated; and P, poorly differentiated.
[b] A, alive; and D, dead.

Please cite this article as: Nishimura T, et al, Proteomic analysis of laser-microdissected paraffin-embedded tissues: (2) MRM assay for stage-related proteins upon non-metastatic lung adenocarcinoma, J Prot (2009), doi:10.1016/j.jprot.2009.11.010

(CE) was determined using the equation: $CE = 0.044 \times m/z + 6$ for doubly-charged precursor ions.

2.3. Construction of candidate MRM assays

Peptides for MRM validation were selected with reference to the results of the previous study using spectral counting, including napsin-A, calgranulin B (S100-A9), hAG-2, peptidyl-prolyl cis-trans isomerase B (PPIase), dermcidin, and periostin [12] (Table 2). Individual peptides were determined empirically using data obtained in the tissue shotgun LC-MS/MS experiments [12] and were used as inputs to MIDAS [10,11] to design MRM assays for proteins characterizing stages IA and IIIA cases (Table 2). Fig. 2 shows two examples of MS/MS spectra of the targeted peptide ions measured by LTQ linear IT mass spectrometer: A) FAIQYGTGR (+2) (*m/z* 506.8) for napsin-A, and B) IMFVDPSLTVR (*m/z* 639.3, +2) for hAG-2. Daughter ions denoted by the arrows were used to design the MRM transitions. Since fragmentation profiles in the LTQ linear IT mass spectrometer generally differ from those in the 4000QTRAP hybrid triple quadrupole/linear IT mass spectrometer, MRM transitions for candidate peptides were evaluated using a 4000QTRAP instrument. Most peptide candidates were selected for lengths of 7–16 amino acids and a +2 peptide charge state.

2.4. Selection of internal standard for MRM measurement

Laser microdissection of tumor cells results in very small amounts of protein that are insufficient for conventional protein assays. Total amounts of proteins and/or peptides usually differ among individual patients. The peptide AGFAGDDAPR (+2, *m/z* 488.7) in the first line of Table 2 is the doubly-charged actin-β peptide and its specific MRM transition to the singly charged fragment (*m/z* 630.3, y6) is utilized as the internal standard. This internal standard is referred to as the in-sample internal standard (ISIS) since actin-β is a housekeeping protein and is shown to be highly expressed in NSCLC cells with minimum variation in semi-quantitative spectral counting analyses [12]. All other peptide MRM measurements were normalized to that for ISIS of 500,000.

2.5. Assessment of MRM measurements

Table 2 summarizes analytical variations for quadruplicate measurements of MRM peak areas for each target peptide using pooled samples, i.e., mixtures of equal volume aliquots of all patient samples. Fig. 3 shows typical MRM mass chromatograms for target peptides. Individual MRM transitions were integrated using the IntelliQuant algorithm in Analyst 1.4.2 (Applied Biosystems). After normalization with ISIS, the median %-CV for all peptide candidates was 12.5% with a range of 2.1–15.8%, except for S100-A9 MRM transitions using VIEHIMEDLDTNADK (+2), which had a very high %CV (Table 2).

3. Results and discussion

3.1. MRM quantitation and validation

The dynamic range of our MRM measurements was examined by spiking tryptic digests of bovine serum albumin (BSA) into peptide mixtures prepared from whole yeast proteins (100 fmol/μL). Twenty MRM transitions for BSA were selected, and the calibration curves for all transitions over the concentration range of 0.032–100 fmol/μL BSA peptides were assessed for quantitative reproducibility (four replicates). Those curves were linear within the range of 0.064 to 200 fmol. The correlation coefficients for all lines were confirmed to be greater than 0.99.

We used an internal standard for quantitative normalization. The specific MRM transition for the doubly-charged actin-β peptide (*m/z* 488.7→*m/z* 630.3, y6) was used as an

Table 2 – Peptide MRM transitions for targeted proteins and their quantitative assessments.

Number	Proteins	Statistical judgements[12]) (Spectral counting)	Peptide sequence (charge state)	Mascot ion score (average*)	MRM transition : [parent ion (*m/z*)/ fragment ion (*m/z*) (ion type)]	Quantitative assessment: %- CV peak area (*n*=4)
1	Actin-β		AGFAGDDAPR (+2)	69.8	488.7/630.3 (y6)	(Internal standard)
					488.7/701.3 (y7)	2.09
2	Napsin-A	IA	FAIQYGTGR (+2)	52.5	506.8/553.3 (y5)	7.91
					506.8/681.3 (y6)	6.06
3	S100-A9	IIIA	VIEHIMEDLDTNADK (+2)	63.2	872.5/776.4 (y7)	>50
					872.5/1151.5 (y10)	>50
4	hAG-2	IIIA	IMFVDPSLTVR (+2)	54.1	639.3/672.4 (y6)	15.79
					639.3/787.4 (y7)	7.6ZY5
5	PPIase	borderline, but significant for IIIA	VLEGMEVVR (+2)	59.1	516.3/690.4 (y6)	13.41
					516.3/e819.4 (y7)	9.67
6	Dermcidin	borderline, but insignificant	ENAGEDPGLAR (+2)	64.1	564.8/628.3 (y6)	5.96
					564.8/814.4 (y8)	11.67
7	Periostin	IIILA	AAAITSDILEALGR (+2)	89.2	700.9/771.5 (y7)	15.32
					700.9/1074.6 (y10)	9.58

Swiss-Prot accession numbers: 1, P60709; 2, Q96009; 3, P06702; 4, Q95994; 5, P23284; 6, P81605; and 7, Q15063.

* Averaged ion scores of peptide sequences used for MRM measurements and were identified by all exploratory LC-MS/M experiments (Ref. [12]).

Please cite this article as: Nishimura T, et al, Proteomic analysis of laser-microdissected paraffin-embedded tissues: (2) MRM assay for stage-related proteins upon non-metastatic lung adenocarcinoma, J Prot (2009), doi:10.1016/j.jprot.2009.11.010

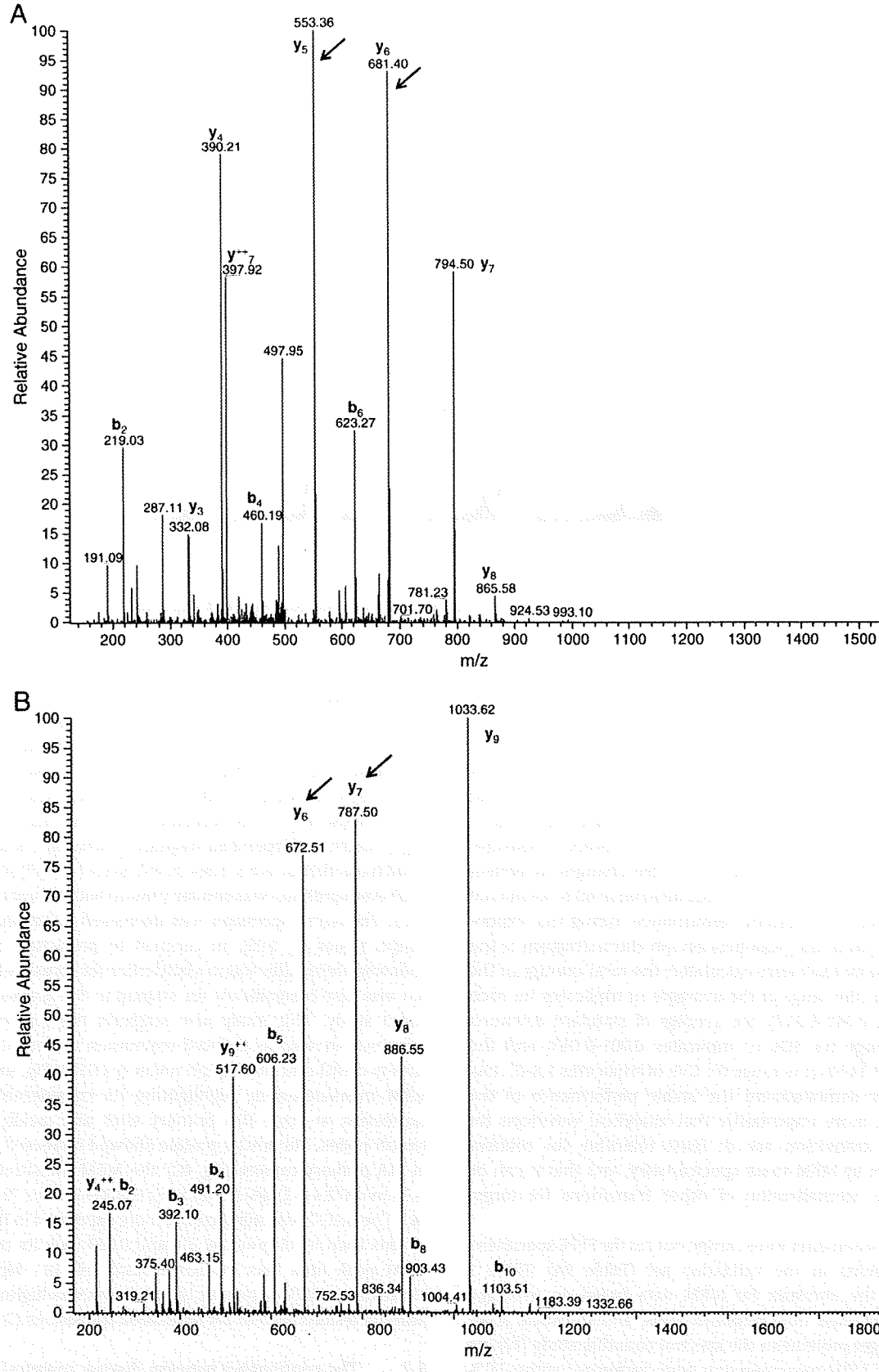

Fig. 2 – Examples of MS/MS spectra of the targeted peptide ions measured by LTQ linear IT mass spectrometer: A) FAIQYGTGR (+2) (*m/z* 506.8) for napsin-A, and B) IMFVDPSLTVR (*m/z* 639.3, +2) for hAG-2. Their MRM transitions were designed by taking into account those fragment y-ions (denoted by the arrows) and transitions recommended *in silico* by MIDAS software that would estimate useful fragment y-ions on an ABI 4000-Qtrap mass spectrometer.

Please cite this article as: Nishimura T, et al, Proteomic analysis of laser-microdissected paraffin-embedded tissues: (2) MRM assay for stage-related proteins upon non-metastatic lung adenocarcinoma, J Prot (2009), doi:10.1016/j.jprot.2009.11.010

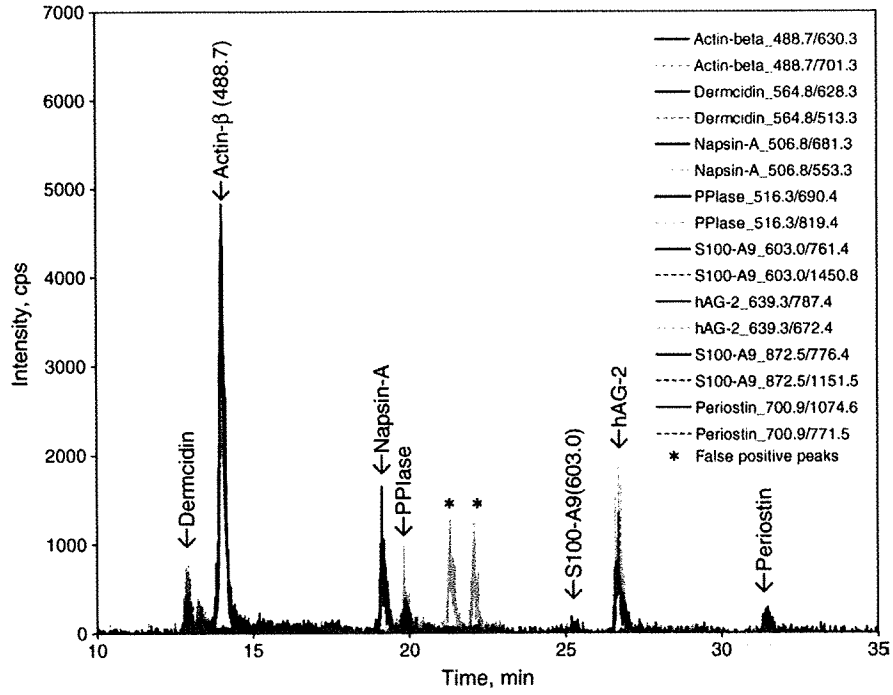

Fig. 3 – A typical MRM mass chromatogram measured for targeted peptides.

internal standard throughout this study. We first examined the run-to-run and sample-to-sample stability of MRM acquisition for this transition, using FFPE sections of approximately equal areas dissected by LMD from stage IA patients. Three aliquots from each patient were measured in the random sequence, and tryptic digests of bovine serum albumin, and mixtures of equal volumes of all FFPE samples were measured every 7 measurements of FFPE aliquots to detect possible changes in system performance. In over a total of 56 samples run in 60 h, we did not encounter decreased system performance during this experiment. The ratios of the peak area on ion chromatogram to the area dissected by LMD were calculated: the total average of the ratios was 0.1 (the range of the averages of triplicates for each FFPE sample, 0.041–0.217), the average of standard deviation 0.015 (the range for SDs of triplicates 0.001–0.043) and the average of CV 14.5% (the range for CVs of triplicates 1.3–37.1%). These results demonstrated the stable performance of the system used, more importantly that analytical variations for this actin-β transition are at least tolerable for relative quantification by MRM mass spectrometry, and that it can be used for the normalization of other transitions for target peptides.

MRM measurements were carried out for the FFPE specimens from 13 patients in the validation set (Table 1A). Table 3 summarizes the statistics for MRM data based on averaged peak areas obtained from duplicate runs, and statistical judgments on target proteins in the spectral counting study [12] are given. Most of MRM measurements were performed within 20 % CV (Table 2). Napsin-A was found to decrease in stage IIIA primary lesions, while it was highly expressed in stage IA (Table 3). S100-A9 seems to be expressed more at stage IIIA but it is difficult to elucidate a conclusion due to its low MRM intensities. hAG-2 was highly expressed at stage IIIA primary lesions (Table 3). PPIase was highly expressed at both stages IA and IIIA. Dermcidin was not statistically significant for either stage IA or IIIA. Periostin was statistically significant for stage IIIA.

PPIase was considered one of the marker candidates specifically expressed in IIIA, but had lower statistical significance; MRM mass spectrometry shows that its expression is high, but did not depend on staging as shown in a boxplot for the MRM transition of m/z 516.3(+2)/m/z 819.4 (+1) (y7) (Fig. 4A). The S100-A9 expression was similarly low in both IA and IIIA primary sites. Periostin expression was decreased at locally advanced lymph nodes ($p<0.05$), in contrast to prediction by spectral counting. Dermcidin was in a borderline for statistical judgment, but was also insignificant for staging in the previous spectral count study. This study also supports the previous results. Napsin-A showed its reduced expression in both IIIA primary sites ($p<0.05$) and IIIA lymph nodes ($p<0.05$). Fig. 4B shows its MRM measurements, highlighting its considerably reduced expression at stage IIIA primary sites and locally advanced lymph nodes. The hAG-2 protein showed increased expression in IIIA primary tumors (Fig. 4C): the MRM transition m/z 639.3 (+2)/m/z 672.4 (+1) (y6) (○) and m/z 639.3 (+2) / m/z 787.4 (+1) (y7) (▲). The hAG-2 was significantly more expressed in IIIA primary lesions than in IA ($p=0.047$ (○) and 0.069 (▲)), its threshold of MRM peak area was located around 2.4×10^5. Moreover, its expression at IIIA metastatic lymph nodes was higher than in IA primary lesions: $p<0.05$ for both MRM transitions (○ and ▲).

3.2. *The relationship between disease prognosis and napsin-A expression levels*

Our MRM measurements showed that the napsin-A levels decreases in stage IIIA, while hAG-2 levels increase in stage IIIA, suggesting for the considerable stage-related nature

Please cite this article as: Nishimura T, et al, Proteomic analysis of laser-microdissected paraffin-embedded tissues: (2) MRM assay for stage-related proteins upon non-metastatic lung adenocarcinoma, J Prot (2009), doi:10.1016/j.jprot.2009.11.010

Table 3 – Summaries of peptide MRM peak areas on candidate proteins measured for IA and IIIA primary sites and locally advanced lymph nodes. Data were subjected to Student T-test and Smirnoff–Grubbs test (both under 5-% significance level) for outlier-data evaluation.

Protein (Swiss-Prot primary accession number)	[Parent ion (m/z)/ fragment ion (m/z)] (ion type)	Average of peak area			Variance			F-value***			p-value			Patient data rejected by the statistical test for outlier data*
		IA	IIIA	IIIAL	IA	IIIA	IIIAL	IA–IIIA	IA–IIIAL	IIIA–IIIAL	IA–IIIA	IA–IIIAL	IIIA–IIIAL	
Anterior gradient protein 2	639.3/672.4 (y6)	68937.8	345816.7	239405.5	7.25E+08	6.63E+10	1.84E+10	91.4	25.3	3.6	0.047	0.030	0.391	6,7
Homolog (hAG-2) (O95994)	639.3/787.4 (y7)	60143.6	236891.8	155657.8	1.59E+09	3.36E+10	6.77E+09	21.1	4.2	5.0	0.069	0.028	0.345	7
Dermcidin (P81605)	564.8/513.3(y5)	82827.9	77903.5	162097.8	1.48E+10	3.44E+09	8.44E+09	4.3	1.8	2.5	0.935	0.249**	0.122	10.13**
	564.8/628.3 (y6)	26261.0	27203.0	54580.9	1.34E+09	4.30E+08	1.13E+09	3.1	1.2	2.6	0.960	0.203	0.160	10,13
Napsin-A (O96009)	506.8/553.3 (y5)	187451.9	32040.7	382.2	1.05E+10	1.90E+09	1.11E+05	5.5	95108.1	17177.4	0.006	0.003	0.135	12**,13**,10**
	506.8/681.3 (y6)	195296.2	27902.6	1543.5	2.47E+10	1.39E+09	4.20E+06	17.7	5879.6	332.0	0.029	0.017	0.145	13**
Periostin (Q15063)	700.9/771.5 (y7)	35008.6	22370.7	9731.4	6.08E+08	4.03E+08	6.26E+06	1.5	97.1	64.4	0.338	0.036	0.187	13**
	700.9/1074.6	3143.6	2214.3	987.8	3.82E+06	4.92E+06	3.50E+05	1.3	10.9	14.0	0.439	0.029	0.241	13**
Peptidyl-prolyl cis-trans Isomerase B (PPIase) (P23284)	516.3/690.4(y6)	23100.3	24446.5	18460.2	1.00E+08	1.68E+08	3.62E+07	1.7	2.8	4.7	0.837	0.344	0.329	
	516.3/819.4 (y7)	51989.8	54865.8	41825.1	5.39E+08	8.52E+08	1.79E+08	1.6	3.0	4.8	0.847	0.366	0.343	
S100-A9 (P06702)	872.5/1151.5 (y10)	32.4	4221.9	57.2	2368	3.05E+07	7464	12889	4089	3	0.122	0.124	0.591	2, 5, 13
	872.5/776.4(y7)	80.6	543.6	0.0	15611	3.10E+05	0	20	–	–	0.102	–	–	10

* Patient number which data rejected according to Smirnoff–Grubbs test (statistical test for outlier data) under 5% significance level.

** Patient's data on lymph node involvement.

*** F-value, the statistical test value regarding to the analysis of variance.

Please cite this article as: Nishimura T, et al, Proteomic analysis of laser-microdissected paraffin-embedded tissues: (2) MRM assay for stage-related proteins upon non-metastatic lung adenocarcinoma, J Prot (2009), doi:10.1016/j.jprot.2009.11.010

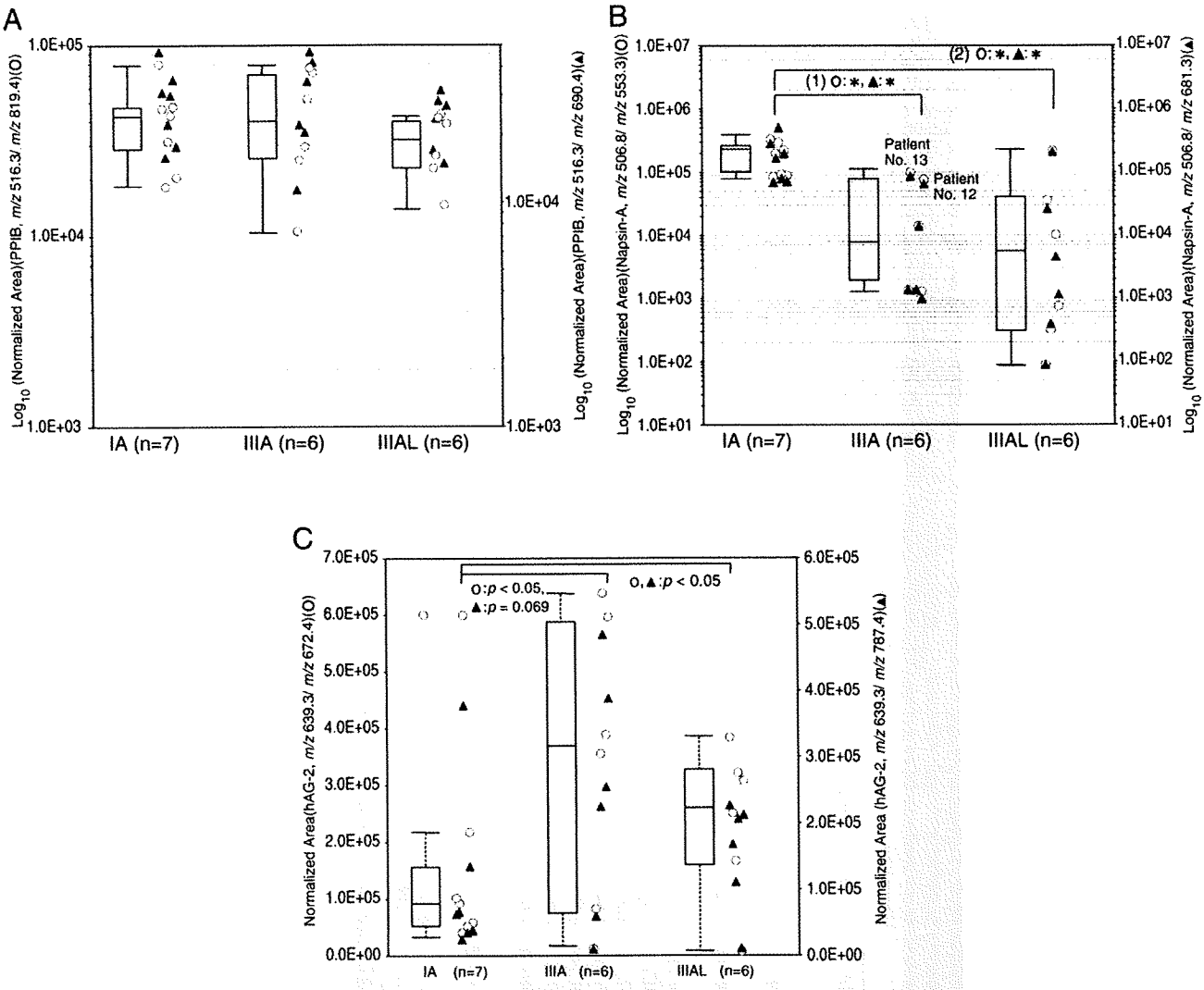

Fig. 4 – MRM measurements for several targeted peptides using samples prepared from the FFPE tissues of the patients from the validation set ($n=13$). Data were plotted as the average of duplicate runs. A) PPIase: the boxplot was given representatively for the MRM measurements, m/z 516.3 (+2)/m/z 819.4 (+1) (y7) (○). B) Napsin-A: the boxplot was given representatively for the MRM transition of m/z 506.8 (+2)/m/z 553.3 (+1) (y5) (○). Significances between IA and IIIA primary sites and also between IA and locally advanced lymph nodes were $^{*}p<0.01$. C) hAG-2: the boxplot was given representatively for the MRM transition m/z 639.3 (+2)/m/z 672.4 (+1) (y6) (○). Significances between IA and IIIA primary sites were $p=0.047$ (○) and 0.069 (▲), and those between IA and locally advanced lymph nodes were $p<0.05$.

of both napsin-A and hAG-2. Close inspection of Fig. 4B, however, reveals that the napsin-A levels of stage IIIA patients 12 and 13 are within the range of those levels in stage IA patients. Those two patients are still alive 33 and 32 months after surgery, while the other patients at stage IIIA died within 20 months after surgery, thereby following the usual prognosis. To explore how the napsin-A levels correlate with disease prognosis, we created an additional patient set (Table 1B) that contained patients with unexpectedly poor or good outcome for a given stage, i.e., the IA-stage patients of poorer prognosis and the IIIA-stage patients of better prognosis. In Table 1B, unusual cases are grouped in the bottom part for each stage. We performed MRM quantification of napsin-A in FFPE specimens from this patient set in the same way as for the validation set. To explicitly express the relationship between the patient's survival time after surgery and the napsin-A levels, the napsin-A MRM peak areas (m/z 506.8/m/z 681.3) are plotted against survival months for all patients in Fig. 5. When the frequency distribution of the peak area values among patients are examined, it can be divided into two parts of the higher and lower values around the value of 4×10^4, which are hereafter denoted by (+) or (–), respectively. Hence, the x-axis for napsin-A is divided at the cutoff value of 4×10^4. The y-axis is divided at 25 months since all the stage IIIA patients of typical outcome died within 23 months after surgery except for patient 22. This two-dimensional map strongly supported the fact that patients with higher expression of napsin-A would be long-term survivors (the good outcome group in the upper right section of Fig. 5) and those with lower expression of napsin-A would be short-term survivors (poor outcome

Please cite this article as: Nishimura T, et al, Proteomic analysis of laser-microdissected paraffin-embedded tissues: (2) MRM assay for stage-related proteins upon non-metastatic lung adenocarcinoma, J Prot (2009), doi:10.1016/j.jprot.2009.11.010

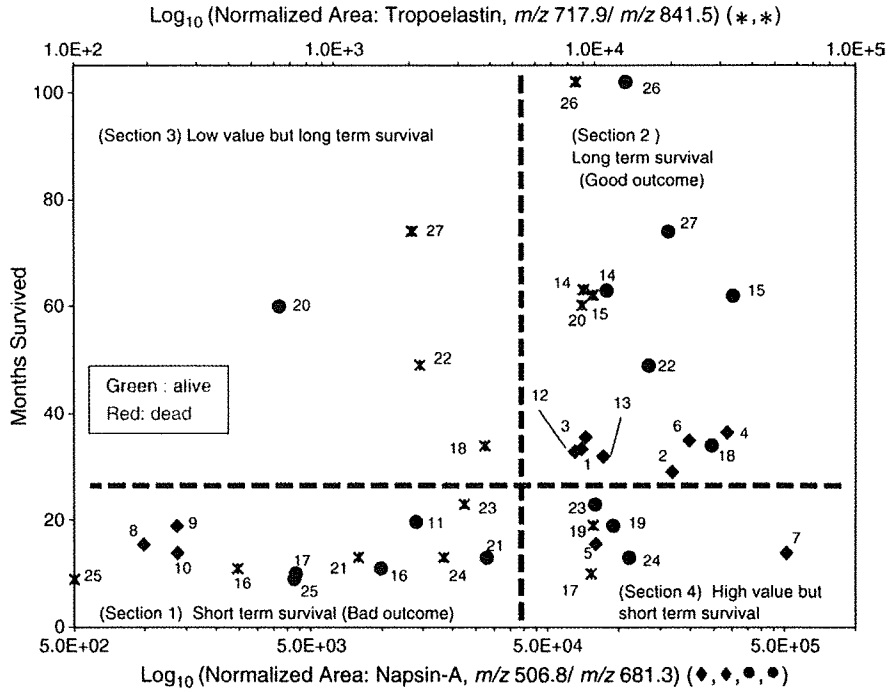

Fig. 5 – A Map of survival months vs. MRM peak areas. MRM transitions used are napsin-A, *m/z* 506.8/*m/z* 681.3 (◊, the validation set of nos. 1–13; ○, the additional patient set of nos. 14–27) and tropoelastin, *m/z* 717.9/*m/z* 841.5 (*, the additional patient set of nos. 14–27). Data points are the averages of duplicate MRM measurements. The patient number is denoted at the corresponding data points. Survival status was indicated by symbols with either green (alive) or red (death). The map is divided into four as described in the text: (Section 1) the short-term survival (poor outcome), (Section 2) the long-term survival (good outcome), (Section 3) the long-term survival but low values, and (Section 4) the short-term survival regardless of high values.

shown in the lower left section of Fig. 5). Like napsin-A, tropoelastin is expressed greatly at stage IA as shown in the previous spectral counting study [12]; the tropoelastin MRM peak areas (transition, *m/z* 717.9/*m/z* 841.5) obtained from the additional patient set are similarly plotted in Fig. 5 with the x-axis division at the value of 5×10^3 (upper x-axis scale). The correlation of the survival time vs. the expression levels of tropoelastin is similar to that for napsin-A.

We then constructed Kaplan–Meier survival curves for napsin-A (+) patients in the Sections 2 and 4 of Fig. 5 ($n=18$) and napsin-A (–) patients in its Sections 1 and 3 ($n=9$), shown in Fig. 6. This clearly demonstrated a significant difference in the survival rate between the two groups ($p=3.27\times10^{-5}$ by a log rank test). The 5-year survivals were 72.2% for napsin-A (+) and 0% for napsin-A (–) patients, respectively.

This study provides evidence that napsin-A and hAG-2 are stage-related secretory proteins. Napsin-A is a member of the aspartic protease family which includes several physiologically important enzymes such as pepsin, chymosin, renin, gastricsin, cathepsin D and cathepsin E [13]. Napsin-A is involved in the processing of surfactant protein B (SP-B) [14]. SP-B is synthesized by type-II pneumocytes as a 42-kDa propeptide (proSP-B), which is posttranslationally processed to an 8-kDa surface-active protein. SP-B is a critical component of surfactant, and a deficiency of active SP-B results in a fatal respiratory failure [15]. Such a functional description of napsin-A persuades us that its expression was significantly reduced at an advanced stage (the IIIA primary lesions and locally advanced lymph nodes) as seen in Fig. 4B, and also that napsin-A expression reflects patient survival (Figs. 5 and 6). Such a variation in napsin-A expression suggests an inverse association between napsin-A and tumor progression and it has been known that lung adenocarcinomas with a low differentiation grade express napsin-A less frequently than highly differentiated tumors [16–18]. The biological properties of hAG-2 in lung cancer have been already discussed in the candidate identification [12].

When we made Kaplan–Meier survival curves for stage IIIA-related hAG-2 similarly to those for napsin-A, and no significant difference was observed between patients with higher and lower hAG-2 levels, unlike napsin-A (data not shown). This would be because the statistical significance level for hAG-2 is considerably higher than that for napsin-A (Table 3). Alternatively, higher hAG-2 levels reflect the ability of cancer to spread to regional lymph nodes (Table 3), but not relate directly to survival duration of stage IIIA patients. We will need to address more patients and further validate hAG-2 as a stage-related biomarker.

4. Conclusion

We demonstrated that FFPE tissue specimens of lung cancer can be used for biomarker MRM MS-based verification. Our MRM quantification demonstrated that napsin-A and hAG-2 were useful for stages IA and IIIA and also related to regional lymph node metastasis, consistent with the results obtained

Please cite this article as: Nishimura T, et al, Proteomic analysis of laser-microdissected paraffin-embedded tissues: (2) MRM assay for stage-related proteins upon non-metastatic lung adenocarcinoma, J Prot (2009), doi:10.1016/j.jprot.2009.11.010

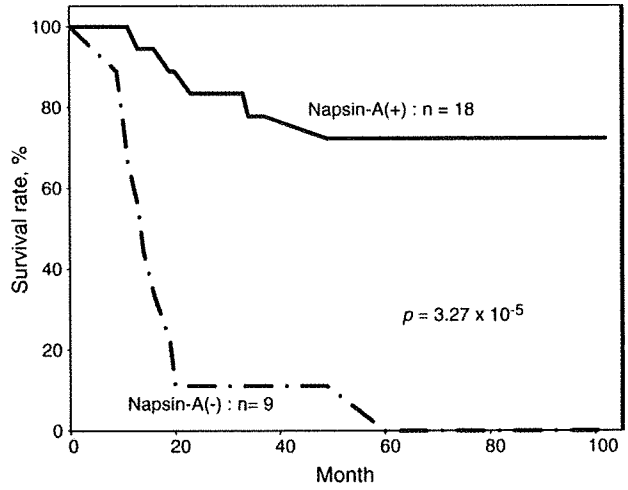

Fig. 6 – Kaplan–Meier curves on survival rates for napsin-A (+) or (–). The log rank test for the difference in survival rate between napsin-A (+) and (–) was $p<0.0001$.

previously by the spectral counting method [12]. The MRM analysis of napsin-A for all patients used here suggested that napsin-A contents correlate with better prognosis in stage IA. In this study it was noted that the stage IIIA cases with good outcome showed the napsin-A profile similar to that of stage IA patients. Thus, MRM-based staging differed from morphology-based staging and might reflect protein expression correlating closely with individual disease outcome. The preceding paper [12] and the verification study demonstrate that direct isolation of tumor cells alone by LMD greatly reduces the complexity of comprehensive analyses, and that MRM mass spectrometry using the endogenous internal standard is a feasible technology for quantitative verification of target proteins in FFPE tissues.

Acknowledgments

We thank Dr. David Krizman (Expression Pathology) for his collaboration, and gratefully acknowledge the financial support from Third Cancer Broad Strategic Project, Japanese Ministry of Public Welfare and Labor. Also we greatly thank Dr. David Hecks (Applied Biosystems) and Mr. Takehito Okada and Ms. Sumie Ando (Applied Biosystems Japan) for their support.

Appendix A. Supplementary data

Supplementary data associated with this article can be found, in the online version, at doi:10.1016/j.jprot.2009.11.010.

REFERENCES

[1] Asamura H, Goya T, Koshiishi Y, Sohara Y, Eguchi K, Mori M, et al. Japanese Lung Cancer Registry study: prognosis of 13,010 resected lung cancers. J Thorac Oncol 2008;3:46–52.

[2] Herbst RS, John V, Heymach JV, Lippman SM. Lung cancer. N Engl J Med 2008;359:1367–80.

[3] Prieto DA, Hood BL, Darfler MM, Guiel TG, Lucas DA, Conrads TP, et al. Liquid Tissue™: proteomic profiling of formalin-fixed tissues. BioTechniques 2005;38:S32–5.

[4] Hood BL, Darfer MM, Furusato B, Lucas DA, Ringeisen BR, Sesterhenn IA, et al. Proteomic analysis of formalin-fixed prostate cancer tissue. Mol Cell Proteomics 2005;4:1741–53.

[5] Hood BL, Conrads TP, Veenstra TD. Unravelling the proteome of formalin-fixed paraffin-embedded tissue. Brief Funct Genomic Proteomic 2006;5:169–75.

[6] Hood BL, Conrads TP, Veenstra TD. Mass spectrometric analysis of formalin-fixed paraffin-embedded tissue: unlocking the proteome within. Proteomics 2006;6:4106–14.

[7] Anderson L, Hunter CL. Quantitative mass spectrometric multiple reaction monitoring assays for major plasma proteins. Mol Cell Proteomics 2006;5:573–88.

[8] Yocum AK, Gratsch TE, Leff N, Strahler JR, Hunter CL, Walker AK, et al. Coupled global and targeted proteomics of human embryonic stem cells during induced differentiation. Mol Cell Proteomics 2008;7:750–67.

[9] McKay MJ, Sherman J, Laver MT, Baker MS, Clarke SJ, Molloy MP. The development of multiple reaction assays for liver-derived plasma proteins. Proteomics Clin Appl 2007;1:1570–81.

[10] Unwin RD, Griffiths JR, Whetton AD. A sensitive mass spectrometric method for hypothesis-driven detection of peptide post-translational modifications: multiple reaction monitoring-initiated detection and sequencing (MIDAS). Nat Protoc 2009;4:870–7.

[11] Cox DM, Zhong F, Du M, Ducoslav E, Sakuma T, McDermott JC. Multiple reaction monitoring as a method for identifying protein posttranslational modifications. J Biomol Technol 2005;16:83–90.

[12] Kawamura T, Nomura M, Tojo H, Fujii K, Hamasaki H, Mikami S, et al., Proteomic analysis of laser-microdissected paraffin-embedded tissues: (1) Stage-related protein candidates upon non-metastatic lung adenocarcinoma. Submitted to be published together in the same volume as the successive articles. J Prot (2009-this volume), doi:10.1016/j.jprot.2009.11.011.

[13] Ueno T, Elmberger G, Weaver TE, Toi M, Linder S. The aspartic protease napsin A suppresses tumor growth independent of its catalytic activity. Lab Invest 2008;88:256–63.

[14] Brasch F, Ochs M, Kahne T, Guttentag S, Schauer-Vukasinovic V, Derrick M, et al. Involvement of napsin A in the C- and N-terminal processing of surfactant protein B in type-II pneumocytes of the human lung. J Biol Chem 2003;278:49006–14.

Please cite this article as: Nishimura T, et al, Proteomic analysis of laser-microdissected paraffin-embedded tissues: (2) MRM assay for stage-related proteins upon non-metastatic lung adenocarcinoma, J Prot (2009), doi:10.1016/j.jprot.2009.11.010

[15] Ueno T, Linder S, Elmberger G. Aspartic proteinase napsin is a useful marker for diagnosis of primary lung adenocarcinoma. Br J Cancer 2003;88:1229–33.
[16] Jagirdar J. Application of immunohistochemistry to the diagnosis of primary and metastatic carcinoma to the lung. Arch Pathol Lab Med 2008;132:384–96.
[17] Chuman Y, Bergman A, Ueno T, Saito S, Sakaguchi K, Alaiya AA, et al. a member of the aspartic protease family, is abundantly expressed in normal lung and kidney tissue and is expressed in lung adenocarcinomas. FEBS Lett 1999;462:129–34.
[18] Dejmek A, Naucler P, Smedjeback A, Kato H, Maeda M, Yashima K, et al. Napsin A (TA02) is a useful alternative to thyroid transcription factor-1 (TTF-1) for the identification of pulmonary adenocarcinoma cells in pleural effusions. Diagn Cytopathol 2007;35:493–7.

Please cite this article as: Nishimura T, et al, Proteomic analysis of laser-microdissected paraffin-embedded tissues: (2) MRM assay for stage-related proteins upon non-metastatic lung adenocarcinoma, J Prot (2009), doi:10.1016/j.jprot.2009.11.010